ADVANCED MATERIALS
www.advmat.de

Omni-Directional Assembly of 2D Single-Crystalline Metal Nanosheets

*Seungyeon Kim, Ho Kwang Choi, Young-Seok Song, Min-Young Seo, Hyunjung Lee, Sukang Bae, Byung Joon Moon, Seoung-Ki Lee, Sang Hyun Lee, and Tae-Wook Kim**

Scalable and cost-effective fabrication of conductive films on substrates with complex geometries is crucial for industrial applications in electronics. Herein, an ultrasonic-driven omni-directional and selective assembly technique is introduced for the uniform deposition of 2D single-crystalline copper nanosheets (Cu NS) onto various substrates. This method leverages cavitation-induced forces to propel Cu NS onto hydrophilic surfaces, enabling the formation of monolayer films with largely monolayer films with some degree of nanosheet overlap. The assembly process is influenced by solvent polarity, nanosheet concentration, and ultrasonic parameters, with non-polar solvents significantly enhancing Cu NS adsorption onto hydrophilic substrates. Furthermore, selective assembly is achieved by patterning hydrophobic and hydrophilic regions on the substrate, ensuring precise localization of Cu NS films. The practical potential of this approach is demonstrated by fabricating a Cu NS-coated capillary tube heater, which exhibits excellent heating performance at low operating voltages. This ultrasonic-driven and selective assembly method offers a scalable and versatile solution for producing conductive films with tailored geometries, unlocking new possibilities for applications in flexible electronics, energy storage, and wearable devices with complex structural requirements.

1. Introduction

Conductive thin films are foundational components in myriad technologies, including flexible electronics, sensors, energy storage devices, and electromagnetic shielding materials.[1–6] The ability to fabricate these films, particularly on substrates with complex geometries or flexible forms, is crucial for the advancement of next-generation electronic devices.[7,8] Traditional methods of depositing conductive films, such as vacuum evaporation, sputtering, and chemical vapor deposition, often require high-vacuum environments and are limited to flat, rigid substrates.[9–15] These constraints hinder the integration of conductive films into flexible or 3D structures, which are increasingly in demand for wearable electronics, soft robotics, and biomedical devices.[16–18]

Solution-based processing techniques — including spin-coating, dip-coating, spray-coating, inkjet-printing, and blade-coating — have emerged as promising alternatives due to their simplicity, cost-effectiveness, and scalability.[19–23] These methods allow for the deposition of conductive materials on a wider range of substrates and are compatible with roll-to-roll manufacturing processes. However, they often face challenges in achieving uniform films, particularly on substrates with arbitrary shapes or non-planar surfaces. While metal nanoparticles, nanowires, and carbon-based materials can be used as solution-processable conductive fillers in these methods, each has drawbacks due to their shapes. These limitations highlight the need for alternative conductive fillers that can overcome these challenges and enable the fabrication of high-performance conductive films on diverse substrates.

S. Kim, H. K. Choi, Y.-S. Song, M.-Y. Seo, H. Lee, T.-W. Kim
Department of Flexible and Printable Electronics
LANL-JBNU Engineering Institute-Korea
Jeonbuk National University
Jeonju 54896, Republic of Korea
E-mail: twk@jbnu.ac.kr

The ORCID identification number(s) for the author(s) of this article can be found under https://doi.org/10.1002/adma.202501632

DOI: 10.1002/adma.202501632

H. K. Choi, S. Bae, B. J. Moon
Functional Composite Materials Research Center
Institute of Advanced Composite Materials
Korea Institute of Science and Technology
Jeollabuk-do 55324, Republic of Korea

S. Bae, B. J. Moon, T.-W. Kim
Department of JBNU-KIST Industry-Academia Convergence Research
Jeonbuk National University
567 Baekje-daero, Deokjin-gu, Jeonju 54896, Republic of Korea

S.-K. Lee
School of Materials Science and Engineering
Pusan National University
2, Busandaehak-ro-63-beon-gil, Geumjeong-gu,
Busan 46241, Republic of Korea

S. H. Lee
School of Chemical Engineering
Chonnam National University
77 Yongbong-ro, Buk-gu, Gwangju 61186, Republic of Korea

Recently, 2D nanomaterials have attracted significant attention due to their unique structural properties and electrical, optical, and mechanical characteristics.[24–28] The representative 2D materials such as graphene, transition metal dichalcogenides, and metallic nanosheets, have shown great potential in electronics, photonics, catalysis, and energy devices.[29–32] Specifically, 2D metal nanosheets of metals such as gold, silver, and copper have been investigated for their excellent electrical conductivity and large surface area.[33,34] Copper nanosheets (Cu NS) are particularly appealing because of copper's high electrical conductivity, abundance, and low cost.[35] The large lateral dimensions and atomic thickness of 2D Cu NS allow them to form continuous conductive networks with fewer junctions, which can enhance electrical performance.[33,34,36,37] Their planar geometry enhances contact with substrates, potentially improving adhesion and film uniformity, compared with lower-dimensional copper-based metallic fillers. Although 2D metallic nanosheets possess numerous advantages as innovative solution-processable conductive fillers, conventional solution-based printing cannot fully harness their dimensional uniqueness. This limitation restricts the fabrication of diverse film architectures and hinders the realization of their full potential. This creates a pressing need to develop novel processes that enable the fabrication of thin films on various substrates, leveraging the unique properties of 2D nanosheets to achieve high-performance conductive films.

Ultrasonication is widely used in nanomaterial processing to disperse particles, exfoliate layered materials, clean substrates, and degas liquids.[38–42] The technique involves applying high-frequency sound waves (typically 20 kHz to several MHz) to a liquid medium, inducing acoustic cavitation, which is the formation, growth, and implosive collapse of microbubbles in liquid.[43] The collapse of these bubbles generates localized high temperatures and pressures, leading to physical and chemical effects that can influence particle behavior.[43,44] Additionally, the implosion of bubbles near solid surfaces produces high-speed microjets and shockwaves, which can influence particle behavior and fluid dynamics.[45] However, the potential of ultrasonication to control assembly of nanomaterials on substrates has not been fully explored.

In this work, we present a novel and versatile method for the omni-directional assembly of 2D single-crystal Cu NS onto substrates of arbitrary shapes and dimensions using ultrasonication. This approach was inspired by an unexpected observation: during ultrasonication of Cu NS dispersion in a glass vial, a shiny metallic film formed on the inner walls. This phenomenon suggested that cavitation induced by ultrasonic waves could facilitate uniform and simultaneous assembly of conductive nanosheets onto surrounding surfaces. We systematically investigated the assembly behavior by examining the roles of solvent polarity, substrate surface energy, ultrasonication time, and nanosheet concentration. The assembly process is governed by the interplay between the hydrophobic nature of the copper nanosheets, the hydrophilic nature of the substrate surface, and the choice of solvent. To demonstrate the versatility and practical applicability of our method, we fabricated a tube-shaped resistive heater by assembling Cu NS on a glass capillary, achieving excellent heating performance at low voltages.

Our findings provide new insights into the mechanisms of ultrasonic-driven assembly of 2D metal nanosheets and introduce a scalable technique for fabricating conductive films on substrates with complex geometries. This opens opportunities for integrating 2D metal nanomaterials into advanced electronic devices and functional coatings where traditional deposition methods are inadequate.

2. Results and Discussion

As a conductive filler, the 2D single-crystal copper nanosheets were synthesized by a conventional hydrothermal method.[33,34,46] After purification, triangular or truncated triangular-shaped nanosheets with an average edge size of 7 μm and a thickness of ≈30 nm were obtained (Figure S1, Supporting Information). Compared with conventional low-dimensional metal nanomaterials (e.g., nanoparticles or nanowires), our 2D metal nanosheets allowed us to cover a desired substate with large area due to the sheets' structural uniqueness in terms of dimension. To assemble 2D metal nanosheets on a desired substrate, we carefully prepared a substrate through a typical ultrasonic cleaning process followed by subsequential dipping of the substrates in prepared solvents, such as acetone and isopropyl alcohol (IPA). Immediately after careful drying in a convection oven, ultraviolet (UV) ozone treatment was carried out to modify the interfacial property and further remove organic residues on the substrate. Because we used a conventional glass or thermally growth silicon dioxide on silicon (SiO_2/Si) substrate with an atomically flat surface, the surface property of the substrates became hydrophilic after cleaning, which is indicative of a high surface energy.

To create conductive metallic thin films on substrates with arbitrary shapes and dimensions using solution-processable techniques, conventional solution-based processing methods such as spin-coating, dip-coating, spray-coating, inkjet-printing, and blade-coating can be used depending on the type of conductive filler.[33,34,46–55] Our discovery of the omni-directional assembly of 2D metallic nanosheets originated from the observation of an unconventional phenomenon that occurred during the ultrasonication of 2D Cu NS in a glass vial to improve dispersion in a solvent. After a period of ultrasonication, the 2D Cu NS formed a shiny metallic film on the inner wall of the glass vial. Although ultrasonication is widely used to disperse nanomaterials, exfoliate layered materials, clean substrates, and degas liquids, few attempts have been reported on the simultaneous and omni-directional assembly of conductive fillers on a substrate via acoustic (ultrasonic) waves.

To understand the assembly of 2D Cu NS via ultrasonication, we carried out ultrasonic-driven assembly of various copper nanocrystals with different dimensions including 0D copper nanoparticles (0D Cu NPs), 1D copper nanowires (1D Cu NWs), and 2D Cu NS onto a glass substrate, as shown schematically in **Figure 1A**. Figure 1B shows photographic images of the substrate, a schematic diagram, and scanning electron micrograph (SEM) images after ultrasonic-driven assembly of 0D, 1D, and 2D copper nanocrystals. The ultrasonic processed glass substrates with both 0D Cu NPs and 1D Cu NWs did not show any assembly or adhesion on the substrate after ultrasonication process. Although some particles and nanowires remained after the process, the appearance was relatively random and no uniform or controllable assembly was visible on the substrate, as shown in the SEM images. However, the apparent change in the color of the

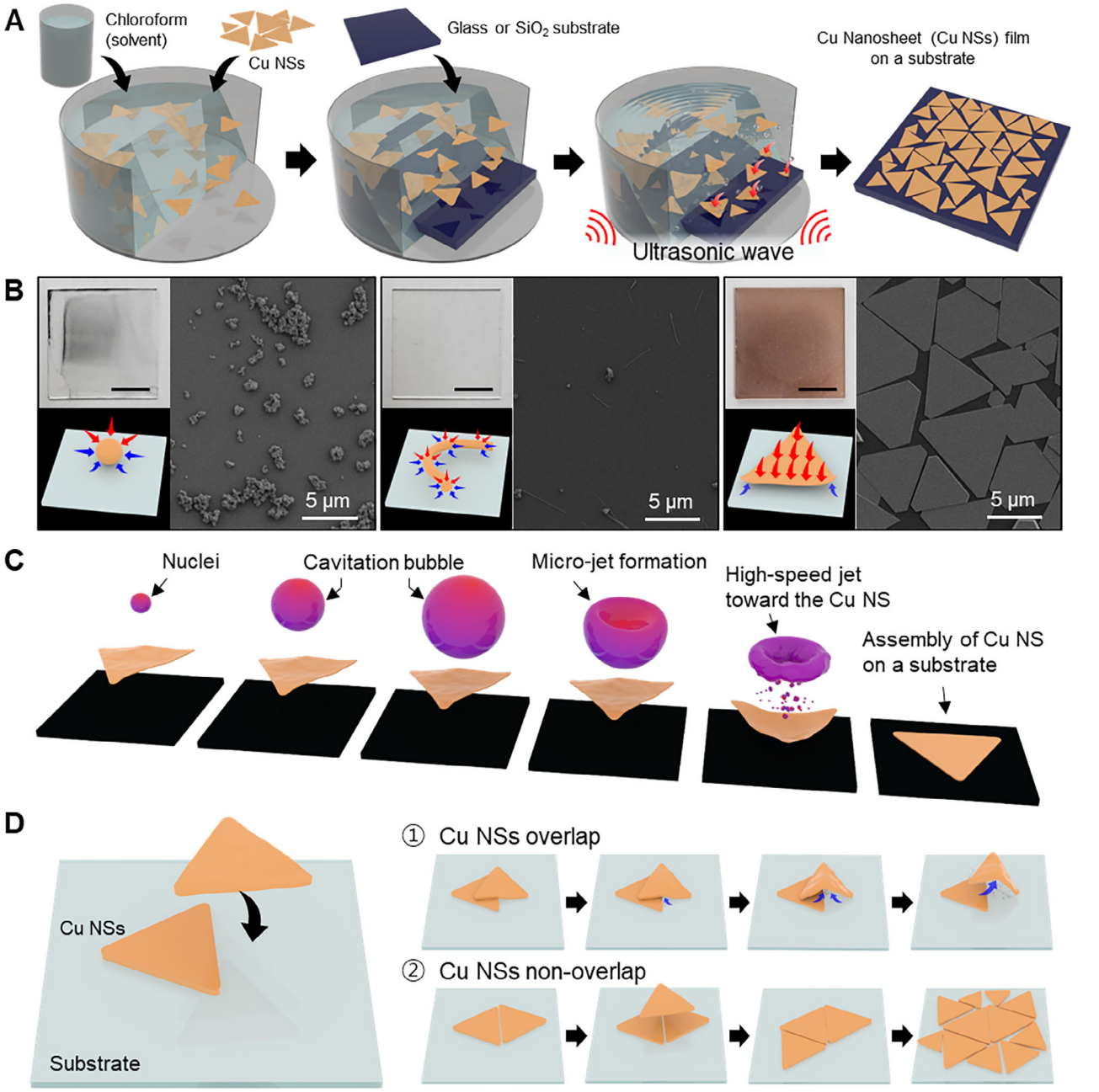

Figure 1. Ultrasonic-driven assembly of copper nanosheets. A) A schematic of the ultrasonic-driven assembly process. Ultrasonic waves generate cavitation bubbles in the solvent, which collapse and produce microjets that propel copper nanosheets toward the substrate, facilitating uniform deposition. B) Comparison of copper nanostructures after ultrasonication. SEM images, photographs, and schematic diagrams of copper nanoparticles (0D), copper nanowires (1D), and copper nanosheets (2D) on substrates post-ultrasonication; inset shows a scale bar of 5 mm. The 2D copper nanosheets exhibit superior substrate coverage and uniformity compared to their 0D and 1D counterparts. C) Cavitation formation and influence of acoustic forces. Schematic representation of cavitation bubble formation during ultrasonication and the resulting acoustic forces acting on the 2D metal nanosheets. D) Possible assembly scenarios under ultrasonication. Schematic diagrams illustrating two different outcomes: (①) overlapping cooper nanosheets leading to non-uniform assembly and lift-off, and (②) well-assembled, non-overlapping copper nanosheets resulting in uniform monolayer films.

transparent glass substrate into a reddish copper implied the assembly of 2D Cu NS on the glass substrate. We found that 2D Cu NS was uniformly coated on the substrate without serious overlap of 2D Cu NS on each other, implying a monolayer assembly of copper nanocrystals with 2D characteristics. Considering conventional ultrasonication, which has been used to clean desired substrates, microscopic bubbles generated by the ultrasonic wave in the solution are considered key to the assembly of 2D Cu NS or the de-assembly of 0D Cu NPs as well as 1D Cu NWs on the substrate. Generally, as an ultrasonic wave travels

through a solution, cavitation bubbles are nucleated by impurities or small undissolved gas bubbles in the liquid. Cavitation involves repeated cycles of rarefaction and compression, leading to rapid collapse.[56–58]

Figure 1C is a schematic of the cavitation that occurs in the 2D Cu NS mixture solution. As depicted in the schematic, when cavitation collapse occurs on or near a solid surface, the solid surface provides resistance to the liquid flow, resulting in asymmetric collapse. Liquid flows into the collapsed cavity from the sides, leading to high-speed jetting of the liquid toward the surface.[58–60] When cavitation collapse occurs in a mixture containing a substrate and Cu NS, the influx of liquid is obstructed by the Cu NS, resulting in the formation of microjets directed toward the Cu NS, causing them to be expelled at high speed. Numerous cavitation collapses occur in the direction of the Cu NS in the mixture solution, propelling the Cu NS toward the substrate and resulting in their assembly on the substrate. The 2D Cu NS appears to be well-placed on the substrate, making 2D contact between the basal plane of the Cu NS and the substrate surface, implying the formation of van der Waals bonds. Although van der Waals forces are relatively weak in nature, the large surface area of Cu NSs is considered to enhance these interactions to a meaningful extent, thereby facilitating more effective contact between the nanosheets and the substrate.[61,62] As a results, Cu NS are closely attached on the substrate after assembly. Negligible pores or gaps form between the Cu NS and the substrate, implying limited creation of microbubbles between the 2D Cu NS and the substrate, preventing disassembly of the Cu NS from the substrate. Due to this cavitation effect, the ultrasonic-driven assembly is superior when the ultrasonic output has a high intensity (40 kHz, 100%), showing ≈82% surface coverage (Figure S2, Supporting Information). This suggests that film formation through ultrasonic assembly is a suitable method for 2D metal nanosheets.

We successfully fabricated a uniform monolayer Cu NS film on a glass substrate measuring up to 2.5 cm × 2.5 cm (Figure S3, Supporting Information). When 0D Cu NPs or 1D Cu NWs are placed on the substrate, they form point and line contacts, respectively. Because cavitation can occur wherever liquid is present during ultrasonication, solid objects on the substrate are subject to omni-directional forces. As 0D Cu NPs are spherical, they are also subject to cavitation forces from all directions. As a result, 0D Cu NPs float on the substrate and return to the solution, making it difficult for them to settle on the substrate. Even after attachment, the contact area between the substrate and the NPs is minimal, allowing cavitation to push the NPs away from the substrate. Likewise, thin and elongated 1D Cu NWs have a small contact area with the substrate that is not sufficient to form van der Waals bonds with the substrate. Even if a force due to cavitation by ultrasonic waves is applied, it does not help anchor them to the substrate, but lifts them toward the solution. The 1D Cu NWs also cannot be attached to the substrate and return to the solution, resulting in ineffective assembly via ultrasonic waves.

The assembled 2D Cu NS on the substrate formed uniform and mostly monolayered metallic thin films on the substrate, as shown in the rightmost SEM image of Figure 1B. This is comparable to what happens during the self-assembly of molecules in solution. Molecular assembly is governed by strong chemical bonds between anchored molecular groups and the substrate. Initially, the molecule has a chance to be absorbed onto the desired surface. It then fills the voids in the substrate, meaning that the molecule is more likely to bind to the substrate than to stay on the assembled molecular forest.[63,64] Cavitation collapse is one of the strong driving forces moving 2D Cu NS from solution to the substrate. Cu NS are then placed on the substrate at the initial stage during ultrasonication. Where the next Cu NS is going to be placed on the substrate should be considered, as shown in Figure 1D. For example, when two Cu NS are present in the system, assuming the first sheet is initially attached to the substrate, the next sheet would preferentially assemble in a manner such that it tries to fill the empty area of the substrate rather than overlap with an existing sheet. When a new sheet is overlaid on an existing sheet and a substrate, a solvent may exist in the gap between the existing sheet and the newly overlaid sheet on the substrate. Cavitation in the gap leads to desorption of overlapping Cu NS from substrate, hindering the stable assembly of new Cu NS. However, if a new sheet is placed on the substrate without overlapping the former sheet, the cavitation force would apply a stronger downward force, which enables van der Waals bonding between the substrate and the Cu NS. In the presence of a large quantity of Cu NS in solution, they preferentially assemble on the empty surface of the substrate, leading to the pseudo-self-assembly of a 2D monolayer film of Cu NS. This behavior, unlike traditional film-formation methods (vortex-mixing, dipping, drop-casting, spray, etc.), enables the uniform assembly of Cu NS across the entire substrate (Figure S4, Supporting Information).

To reveal the specific assembly process of 2D metallic nanosheets via ultrasonic waves, we focused on the relationship of the three major components in the system: the solvent, nanosheet and substrate). As shown in Figure 1, we found that the assembly of metallic nanocrystals strongly depends on the contact area between matters and substrates. Because cavity collapse in a Cu NS solution induces the attachment of 2D metal nanosheets to substrates but does not lead to chemical bonding, ultrasonic-driven assembly of Cu NS requires an investigation of the correlation among the substrate, Cu NS, and solvent. Generally, nanoparticles have strong electrostatic interaction between them, resulting in irreversible aggregates in water.[65,66] Surface-capping molecules have been introduced to allow enhanced electrostatic stabilization in a solvent. For example, a ligand such as polyvinylpyrrolidone enables the dispersion of nanoparticles in polar solvents due to their hydrophilic functional groups; this can be difficult in non-polar solvents.[67] In the case of Cu NS, unlike molecular-level interactions, bulk-scale assembly occurs, making the surface's chemical properties (such as polarity) crucial. The physical characteristics (such as surface roughness) are also believed to significantly influence the assembly process.

Based on an understanding on the relationship between the surface property of nanosheets and polarity of solvents, we carried out ultrasonication of the nanosheets by changing various solvents, specifically n-hexane, toluene, chlorobenzene (CB), chloroform (CF), dichlorobenzene (DCB) and 2-propanol (IPA), acetone (AC), ethanol (EtOH), methanol (MtOH), acetonitrile (ACN), deionized water (DIW), and ethylene glycol (EG), for non-polar and polar solvents (Figure S5 and Table S1, Supporting Information). **Figure 2** illustrates the representative ultrasonic-driven assembly characteristics of Cu NS and fully oxidized Cu NS depending on the polarity of the solvents. As with representative noble metals such as gold and silver, pure metallic

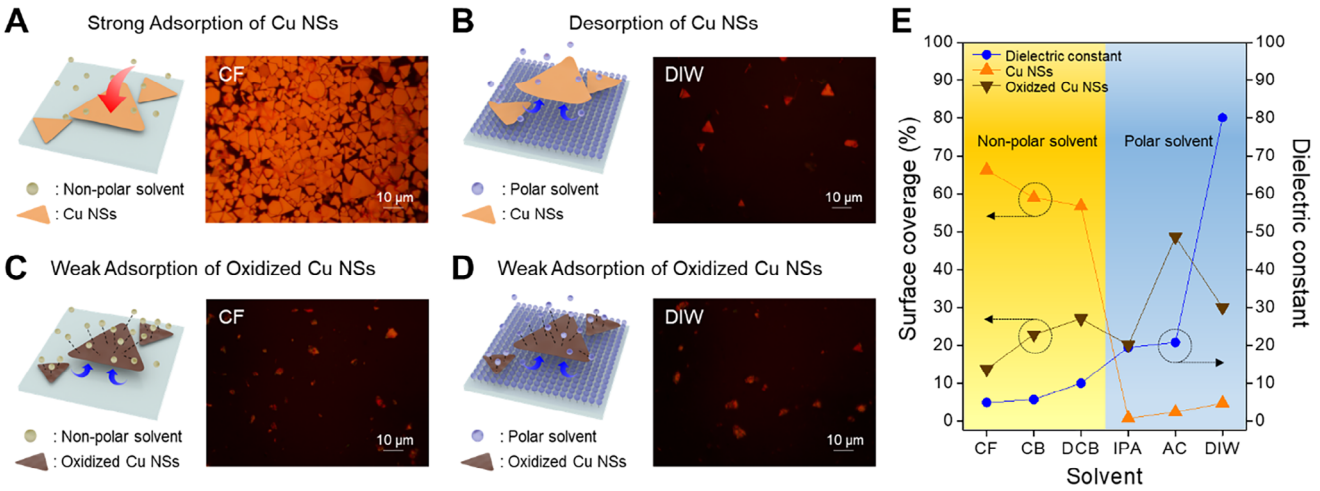

Figure 2. Solvent-dependent assembly of Cu NS and oxidized Cu NS under ultrasonication. A) Strong adsorption of Cu NS in non-polar solvent (CF), in which copper nanosheets remain stable, assembling into a densely packed structure. B) Weak adsorption of Cu NS in polar solvent (DIW). C) Weak adsorption of oxidized Cu NS in non-polar solvent (CF). D) Weak adsorption of oxidized Cu NS in polar solvent (DIW). E) A dielectric constant–dependent phase diagram illustrating the surface coverage of Cu NS versus oxidized Cu NS across representative non-polar (CF, CB, DCB) and polar (IPA, AC, DIW) solvents. The surface coverage is strongly dependent on both the surface state of the nanosheets (oxidized vs. non-oxidized) and the polarity of the solvents, with optimal assembly occurring when non-oxidized Cu NS are assembled in non-polar solvents.

copper has inherently hydrophobic surface characteristics.[67,68] However it is difficult to avoid the chemical bonding of pure copper with oxygen-related moieties; this is responsible for hydrophilic characteristics.[69] Due to its special crystalline structure, our Cu NS, has a basal plane of (111), giving it superior resistance against surface oxidation and allowing for the formation of a smooth Cu_2O phase with intrinsic hydrophobicity.[70–74] The spray-printed Cu NS film exhibited surface properties close to hydrophobic, with a measured contact angle of 107.12° (Figure S1C, Supporting Information). As mentioned previously, the surface status of substrates is one of the important parameters to achieve assembly of Cu NS on a desired substrate. Silanol groups (-SiOH) with a terminated glass substrate possess a hydrophilic nature.[75,76] The high adsorption activity of the surface allows it to adsorb numerous foreign materials in an atmospheric environment, leading to a decrease in surface energy.[77,78] Similarly, the glass substrate with high surface energy achieved after sequential wet cleaning and UV-ozone treatment indicative of a hydrophilic surface. When directly immersed in the Cu NS solution, the glass surface attempts to reduce its high surface energy by the assembly of nearby Cu NS. When ultrasonic waves are applied to a Cu NS solution with a non-polar solvent, it accelerates the adsorption of the hydrophobic Cu NS toward the hydrophilic glass surface instead of staying in non-polar organic solvents (e.g., CF), thereby attempting to lower the surface energy of the substrate, as shown in Figure 2A. Additionally, it is important to consider the influence of crystalline orientation on the surface energy of metals, which in turn affects their interfacial behavior. For instance, it is well established that Cu(110) exhibits higher hydrophilicity than Cu(111), leading to distinct wetting characteristics on metal surfaces.[74] Owing to these differences in surface energy associated with different crystallographic planes, Cu nanosheets with a (111) orientation are expected to provide more favorable conditions for ultrasonic-driven assembly compared to those with a (110) orientation.

To prove our hypothesis, we carried out additional ultrasonic assembly of Cu NS with other representative non-polar organic solvents. We found that this phenomenon is consistent regardless kinds of the choice of solvent, implying preferential absorption of Cu NS on the hydrophilic glass surface (Figure S5 and Table S1, Supporting Information). However, the resulting sheets exhibited a completely opposite behavior under polar solvents, as shown in Figure 2B. Initially, when Cu NS and a hydrophilic glass substrate stay together in a polar solvent, the substrates are expected to be surrounded by polar solvent, which means that polar molecules are preferentially adsorbed on the hydrophilic glass surface.[75,77] During ultrasonication, cavitation on the glass surface becomes more active than in a non-polar solvent due to the adsorbed polar-solvent molecules on the hydrophilic surface.[79,80] Finally, Cu NS are displaced from the hydrophilic substrate and return to the polar solvent, leading to poor assembly of Cu NS on the hydrophilic substrate in the presence of a polar solvent (Figure 2B).

We performed further ultrasonication of the oxidized Cu NS with the glass substrate in both polar and non-polar solvents, as illustrated in Figure 2C,D. Unlike the previously discussed Cu NS, the oxidized Cu NS did not assemble well onto the substrate in either solvent. The main difference between Cu NS and oxidized Cu NS was the oxidation state of the surface. Due to the presence of oxygen at the basal plane of Cu NS, it exhibited more interactions with the hydrogen in the organic solvents regardless of polarity. Moreover, the surface of the oxidized Cu NS was rougher than that of the unoxidized Cu NS, which likely created gaps between the oxidized Cu NS and the substrate after assembly (Figure S6, Supporting Information). These gaps made it difficult to establish strong van der Waals interactions, and the formation of cavitation bubbles within the gaps during ultrasonication further disrupted the assembly, causing the oxidized Cu NS to disassemble from the substrate. As a result, the oxidized

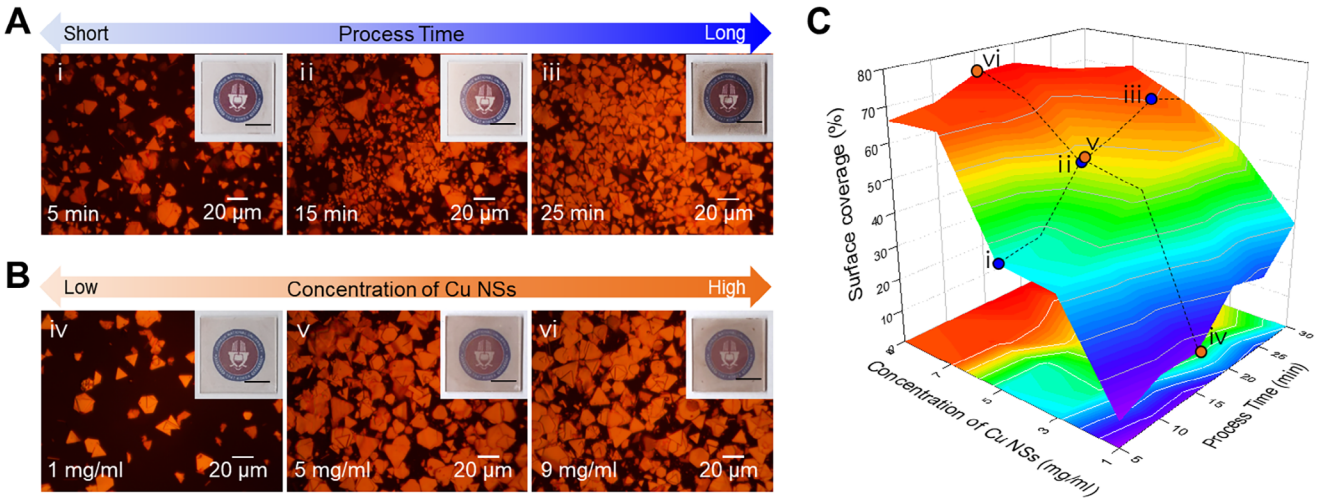

Figure 3. Effect of ultrasonication time and copper nanosheet (Cu NS) concentration on assembly and surface coverage. A) Impact of ultrasonication process time on Cu NS assembly. Optical microscopy images illustrate how varying the ultrasonication time affects the surface coverage of Cu NS. Samples were prepared using a 5 mg mL^{-1} Cu NS dispersion and subjected to ultrasonication for (i) 5 min, (ii) 15 min, and (iii) 25 mins. The surface coverages were approximately (i) 32%, (ii) 58%, and (iii) 77%, respectively. B) Influence of Cu NS concentration on assembly density. Optical microscopy images depict the effect of different Cu NS concentrations on the assembly process, with a constant ultrasonication time of 15 min. Samples were prepared with Cu NS concentrations of (iv) 1 mg mL^{-1}, (v) 5 mg mL^{-1}, and (vi) 9 mg mL^{-1}, resulting in surface coverages of approximately (iv) 22%, (v) 62%, and (vi) 65%, respectively. C) 3D contour plot correlating surface coverage with ultrasonication time and Cu NS concentration. Surface coverage is represented as a function of both variables, highlighting the synergistic relationship between ultrasonication duration and Cu NS concentration.

Cu NS tended to remain in the solvent rather than adhere to the substrate in both non-polar and polar solvents.[81]

While our study primarily attributes the stable assembly of Cu NSs to van der Waals interactions, additional factors may also contribute to their strong adhesion to the substrate. The large surface area of Cu NSs enhances van der Waals forces, but differences in surface energy between Cu NSs and the SiO_2 substrate could further facilitate stable adsorption. Electrostatic interactions arising from charge transfer at the interface may also strengthen adhesion, as previous studies suggest localized dipole formation when Cu NSs come into contact with SiO_2.[82] Furthermore, the ultrasound-induced cavitation effect generates localized high-pressure zones that promote nanosheet attachment,[59] while capillary forces during solvent evaporation may play a role in stabilizing the final assembly.[83] These combined effects suggest that nanosheet adhesion is likely governed by a synergy of multiple interactions rather than van der Waals forces alone.

Based on our understanding of the assembly of Cu NS on a desired substrate, we further studied the degree of Cu NS assembly with respect to processing time and the concentration of the Cu NS solution. To investigate the influence of ultrasonication time, a glass substrate was immersed in a 5 mg mL^{-1} Cu NS solution and ultrasonication was applied for periods ranging from 5 to 30 min, in 5 min intervals. As shown in **Figure 3**A, longer processing times resulted in more Cu NS assembling on the substrate. Specifically, the coverages of the substrate were ≈32%, 40%, 48%, 66%, 71%, and 75% for processing times from 5 to 30 min, in 5 min increments (Figure 3A; Figure S7, Supporting Information). We also identified the concentration-dependent assembly characteristics of Cu NS in the solution, as shown in Figure 3B. By varying the concentration of the Cu NS solution from 1 to 11 mg mL^{-1} in 2 mg mL^{-1} increments, at a fixed processing time of 15 min, we observed distinct differences in surface coverage: ≈22%, 55%, 62%, 67%, 65%, and 57%, respectively (Figure 3B; Figure S8, Supporting Information). These results align closely with the proposed mechanism of monolayer Cu NS assembly on the substrate.

In the initial stages of assembly, the Cu NS were randomly distributed across the substrate. As the process continued, the available area on the substrate decreased, requiring more time to fill the remaining empty spaces. This sequential assembly behavior resulted in a time-dependent assembly phenomenon under ultrasonication. At a fixed processing time, higher concentrations of the Cu NS solution led to greater Cu NS deposition on the substrate, resulting in greater surface coverage within the same period. However, increasing processing times and Cu NS concentrations did not result in a continuous increase in Cu NS assembly. Notably, a slight decrease in surface coverage was observed when the sonication time exceeded 25 min (Figure S8, Supporting Information), suggesting that prolonged exposure to ultrasonic waves may induce detachment or fragmentation of Cu NSs due to excessive cavitation forces. This observation implies that there exists an optimal processing window, beyond which structural degradation of the nanosheets begins to outweigh further assembly. In our experiments, the maximum surface coverage was measured at 88.01%, indicating a practical upper limit for uniform film formation under the given assembly conditions. Additionally, smaller Cu NSs were found to more effectively occupy interstitial spaces on the substrate surface, thereby enhancing overall coverage (Figure S9, Supporting Information). When Cu NSs of varying lateral dimensions were tested, those with an average size of 5 μm achieved a surface coverage of 72.83%, compared to 70.78% for medium-sized nanosheets (8 μm) and 54.43% for larger ones (14 μm). These findings further emphasize the critical role of nanosheet size optimization in improving assembly uniformity and maximizing surface coverage. The

correlations between surface coverage, processing time, and concentration are shown in a contour plot in Figure 3C (with further details supplied in Table S2, Supporting Information). The surface coverage increased with processing time and concentration, indicating that our ultrasonic-driven assembly method allows for precise control of Cu NS surface coverage, which is important for practical applications in conductive metallic films. To further explore the versatility of this approach, we investigated whether the ultrasonic assembly method could be extended to metal nanosheets beyond Cu NSs. Specifically, we conducted additional experiments using Ag NSs, which also exhibit a (111) single-crystal structure similar to Cu NSs. Ag NSs were successfully assembled onto the substrate, confirming the applicability of our technique beyond Cu NSs (Figure S10C,D, Supporting Information). However, under identical ultrasonic conditions, the maximum surface coverage achieved with Ag NSs (38.21%) was markedly lower than that of Cu NSs (88.01%). This difference can be attributed to variations in surface energy and surface roughness. While Ag(111) possesses a lower surface energy (1091.16 mJ m^{-2}) compared to Cu(111) (1408.62 mJ m^{-2}),[84] the Ag NSs exhibited significantly higher RMS roughness (7.150 nm) than Cu NSs (3.339 nm). Increased surface roughness disrupts van der Waals interactions with the substrate, leading to interfacial gaps and reduced adhesion efficiency during ultrasonic assembly. This trend is consistent with our observations in oxidized Cu NSs, where increased roughness hindered effective film formation. These findings highlight the critical influence of surface roughness and surface energy on ultrasonic-driven assembly efficiency, underscoring the need to account for material-specific properties when applying this technique to different metal nanosheets. Moving forward, we are actively expanding our study to include additional metallic nanosheets with diverse crystalline structures and surface characteristics to gain deeper insights into the fundamental mechanisms governing ultrasonic-driven assembly.

To investigate the feasibility of ultrasonic-driven assembly of metallic nanosheets for diverse applications, we conducted additional experiments to study the behavior of metallic nanosheets on various substrate surfaces (**Figure 4**). As discussed earlier, the assembly of Cu NS was highly dependent on the properties of the three major components (solvent, nanosheet, and substrate) and was successfully achieved using a combination of a non-polar solvent, metallic nanosheets, and a substrate with a hydrophilic surface. In preliminary studies on the surface characteristics of substrates, we found that the assembly behavior varied significantly on both hydrophilic substrates (e.g., glass and SiO_2/Si wafer) and hydrophobic substrates (e.g., polyimide [PI] film and Teflon), regardless of solvent choice and the oxidation state of the Cu NS (Figure S11, Supporting Information). These substrates were subjected to ultrasonic waves in AC and IPA, followed by UV-ozone treatment for 5 min. On the superhydrophilic glass and SiO_2/Si, Cu NS assembled uniformly, while on PI films, only minimal amounts of Cu NS assembled or formed as localized films as the solvent evaporated. Because Cu NS assembly depends heavily on surface energy, selective assembly was achieved by altering the surface properties of specific areas on the substrate. To control the surface characteristics, we introduced a phosphonic acid–based self-assembled monolayer (FDDPA) on a sputtered aluminum oxide (AlO_x) thin film, which imparted hydrophobicity, with a contact angle of 118.6°. We then exposed the prepared substrate to UV light (254 nm) and ozone for 5 min using a shadow mask with a rectangular pattern. After UV-ozone treatment, the surface-affected (SAM) monolayer was selectively removed, leaving the AlO_x layer with superhydrophilic characteristics and an indiscernible contact angle (Figure S12, Supporting Information).

To examine the preferential adsorption of Cu NS in relation to surface energy, we subjected the prepared substrate to ultrasonication after immersing it in a mixture of Cu NS and a non-polar solvent (CF), as shown in Figure 4A. The Cu NS selectively assembled on the rectangular areas with strong hydrophilicity due to the UV-ozone treatment, as shown in the lower microscopy images of Figure 4B. As explained earlier, Cu NS adsorbed on the hydrophilic surface, reducing the surface energy of the substrate. In contrast, hydrophobic surfaces did not allow for adsorption of Cu NS due to their low surface energy and higher probability of cavitation compared with hydrophilic surfaces.[85–88]

Our findings are consistent with those of previous reports on the effect of ultrasonic cavitation on hydrophobic and hydrophilic surfaces; gas nucleation occurred primarily on hydrophobic surfaces during the initial stages of ultrasonic treatment.[89] This indicates that hydrophobic surfaces with high contact angles have a lower nucleation barrier, which reduces the energy barrier for gas nucleation. When Cu NS are assembled under hydrophilic conditions, they easily adhere to the substrate with minimal cavitation, promoting film formation. However, under hydrophobic conditions, a high concentration of microbubbles forms on the surface, and when Cu NS are jetted onto the surface, the pressure from cavitation counteracts the attaching force, as illustrated in the upper schematics of Figure 4B.

An ultrasonic wave, a type of acoustic wave, propagates effectively through a liquid medium.[90,91] Based on our experimental setup, when the ultrasonic wave interacts with an individual copper nanosheet, it exhibits no directional preference but instead induces random motion of the Cu NS in the solvent, driven by cavitation forces in an omni-directional manner. While conventional coating processes such as evaporation, sputtering, spray-printing, and inkjet-printing have been used extensively to form conductive thin films, which are essential components in both electronic devices and functional films, these methods are inherently optimized for flat, 2D substrates.[92] However, they often face limitations in achieving uniformity and precision on complex or non-planar surfaces, which restricts their versatility in the fabrication of next-generation devices. Additionally, many of these techniques require vacuum environments or elevated temperatures, further constraining their applicability to flexible or heat-sensitive materials. In contrast, ultrasonic-driven assembly of Cu NSs can easily form conductive films on complex structures such as narrow wires, capillary tubes, and intricate 3D surfaces, as shown in **Figure 5**. For example, a cleaned glass teapot was immersed in a Cu NS solution and exposed to ultrasonic waves. In this process, both the Cu NS and solvent surrounded the teapot in all directions, while cavitation, induced by the ultrasonic waves, occurred throughout the solution, enabling Cu NS assembly even on the sharp curves of the teapot's interior, spout, and handle. After the ultrasonic-driven assembly, the teapot was removed, rinsed with clean CF, and thoroughly dried, resulting in a surface that was densely coated with Cu NS. (Movie S1,

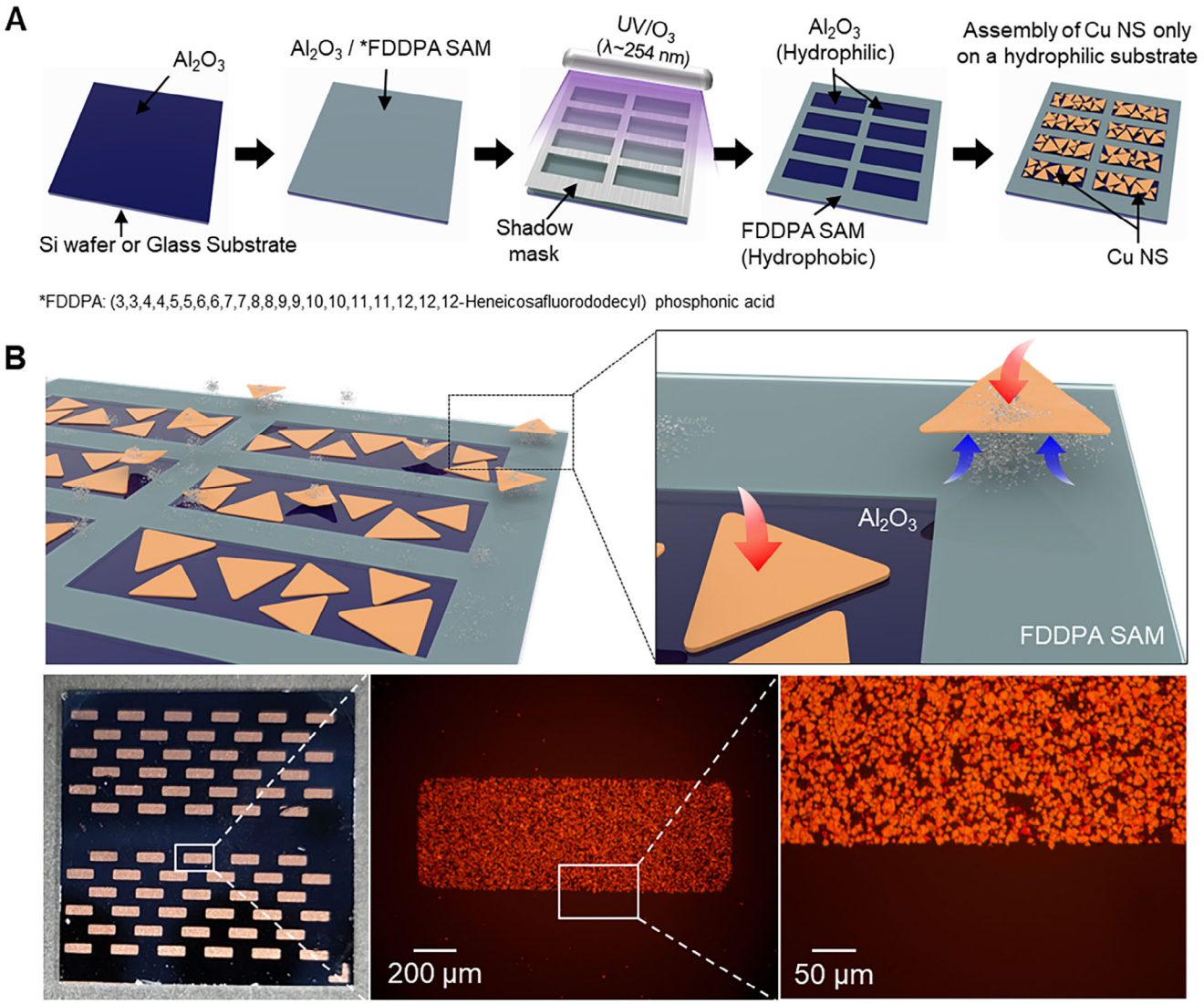

Figure 4. Ultrasonic-driven selective assembly of copper nanosheets (Cu NS) using patterned functionalized surfaces. A) Schematic showing the fabrication steps of a patterned substrate for Cu NS assembly. The process involves the cleaning and preparation of a glass substrate, deposition of aluminum oxide (Al_2O_3) and a self-assembled monolayer (SAM) of FDDPA, and the application of shadow mask to create distinct areas for the targeted assembly of Cu NS B) Schematics of the selective assembly process and optical microscopy images of the patterned substrate with assembled Cu NS. Cu NS are directed to the patterned regions on the substrate, where the SAM removed. The red arrows indicate the forces guiding the Cu NS, while the blue arrows show a lift-off during assembly. The images show the patterned substrate with the densely packed Cu NS within the patterned regions (scale bar: 50 µm).

Supporting Information). Optical microscopy images of the sharply curved entrance further confirmed the dense assembly of Cu NS. As shown in Figure 5B, the successful assembly of Cu NS of various complex shapes, including cubes, pumpkins, and whale figurines, was achieved. The ability to create 3D objects such as dice through ultrasonic-driven assembly, in conjunction with the substrate patterning characteristics mentioned earlier, was also demonstrated. The deposition was successfully carried out on flexible polymer substrates such as polyethylene naphthalate. Such results emphasize the potential of this method to provide a simple and effective way to fabricate conductive films, uniformly coating a variety of substrates with 2D single-crystalline metal nanosheets.

Based on our findings and the assembly characteristics of Cu NS, we fabricated a tube-shaped 3D resistive heater by assembling Cu NS onto a glass capillary tube (**Figure 6**). Omnidirectional deposition made possible by ultrasonic-driven assembly allowed for the formation of conductive films of Cu NS on the outer surface of the capillary tube. To ensure precise assembly, the glass capillary tubes, which were cleaned with AC and IPA, were immersed in the Cu NS solution and both ends were sealed with Teflon tape to prevent deposition on the inner walls of the tube. Figure 6A,B present photographs, optical microscopy, and SEM images of the glass tube before and after Cu NS assembly. For effective electrical conduction, the assembled Cu NS must be closely packed to form efficient electrical contacts

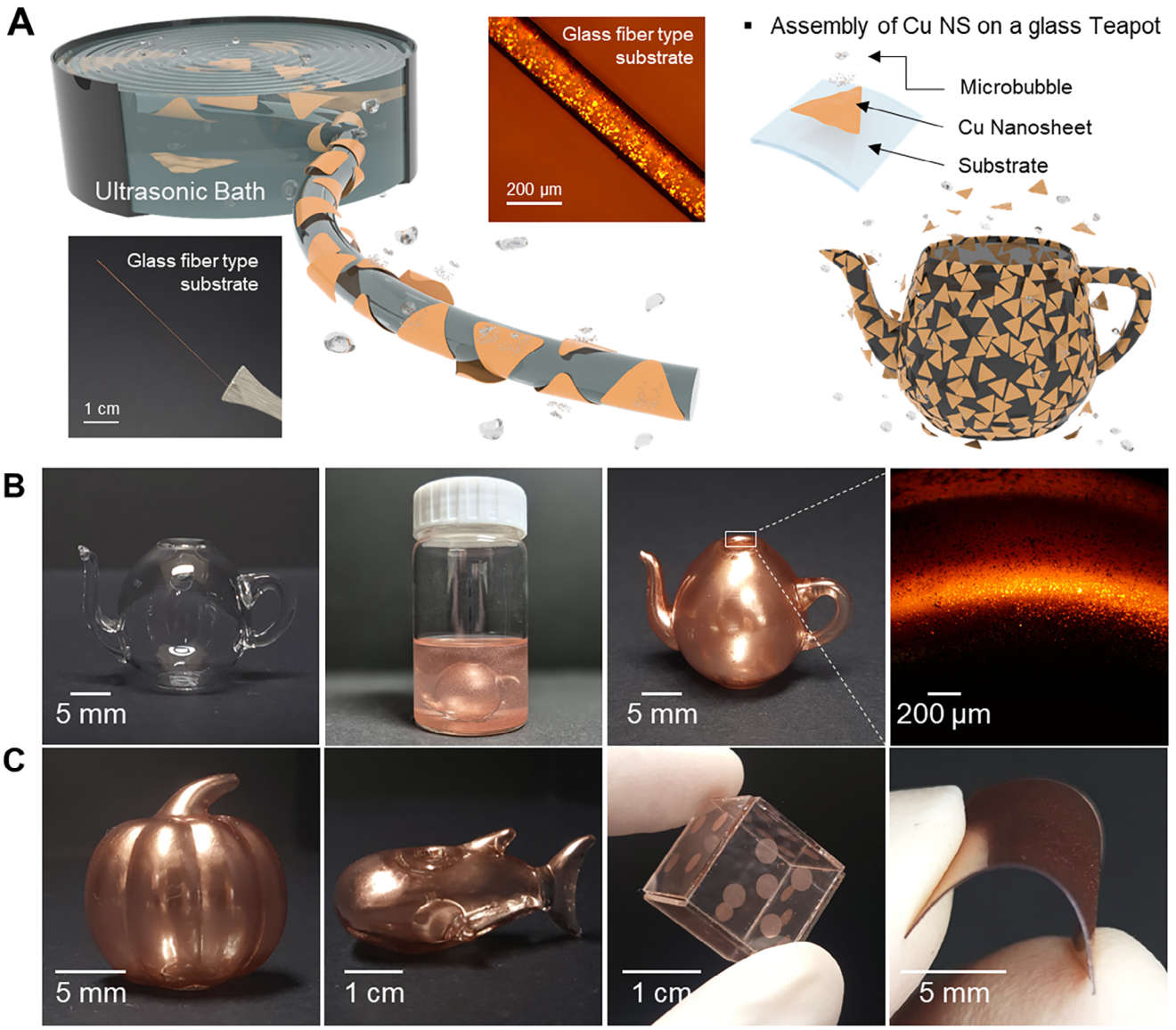

Figure 5. Ultrasonic-driven omni-directional assembly of copper nanosheets (Cu NS) on complex geometries and flexible substrates. A) Schematic of Cu NS deposition on complex 3D structures. The teapot exemplifies the potential for uniformly coating complex 3D surfaces using ultrasonication. B) Photographs of the assembly of Cu NS on various substrates and objects. From left to right: a transparent glass teapot before Cu NS coating, illustrating the original substrate; a vial containing the Cu NS dispersion with the glass teapot submerged during the ultrasonication process; the same teapot after coating, with a uniform layer of Cu NS on its surface. The inset on the right provides a close-up view of the nanosheet coverage. C) Examples of Cu NS–assembled objects demonstrating the versatility of the coating technique. From left to right: A small pumpkin-shaped object, a dolphin-shaped figurine, a glass die with assembled Cu NS, and a flexible copper-coated substrate.

between neighboring nanosheets. After the ultrasonic process, we achieved well-connected, conductive films of Cu NS on the outer surface of the glass capillary tube, with a measured resistance of 128.0 Ω (Figure 6C). To evaluate the heating performance of the tube-shaped resistive heater, we applied a DC bias to both ends of the conductive capillary. We monitored the temperature and captured thermal images using an infrared camera as the applied voltage was increased from 0.5 to 2.5 V over 30 min. Similar to conventional resistive heaters, our device exhibited excellent heating characteristics, achieving temperatures of 24.4, 35.3, 44.8, and 57.0 °C at applied voltages of 1.0 , 1.5 , 2.0 , and 2.5 V, respectively (Figure 6D).

To further analyze the performance of our tube-shaped resistive heater, we systematically examined the temperature distribution as a function of the applied voltage and time, as depicted in the contour plot of Figure 6E (Figure S13, Supporting Information). As the duration of applied voltage increased, the surface temperature of the tube rose steadily, indicating that higher applied voltages accelerated joule heating. The 3D capillary tube heater reached ≈60 °C within 25 min

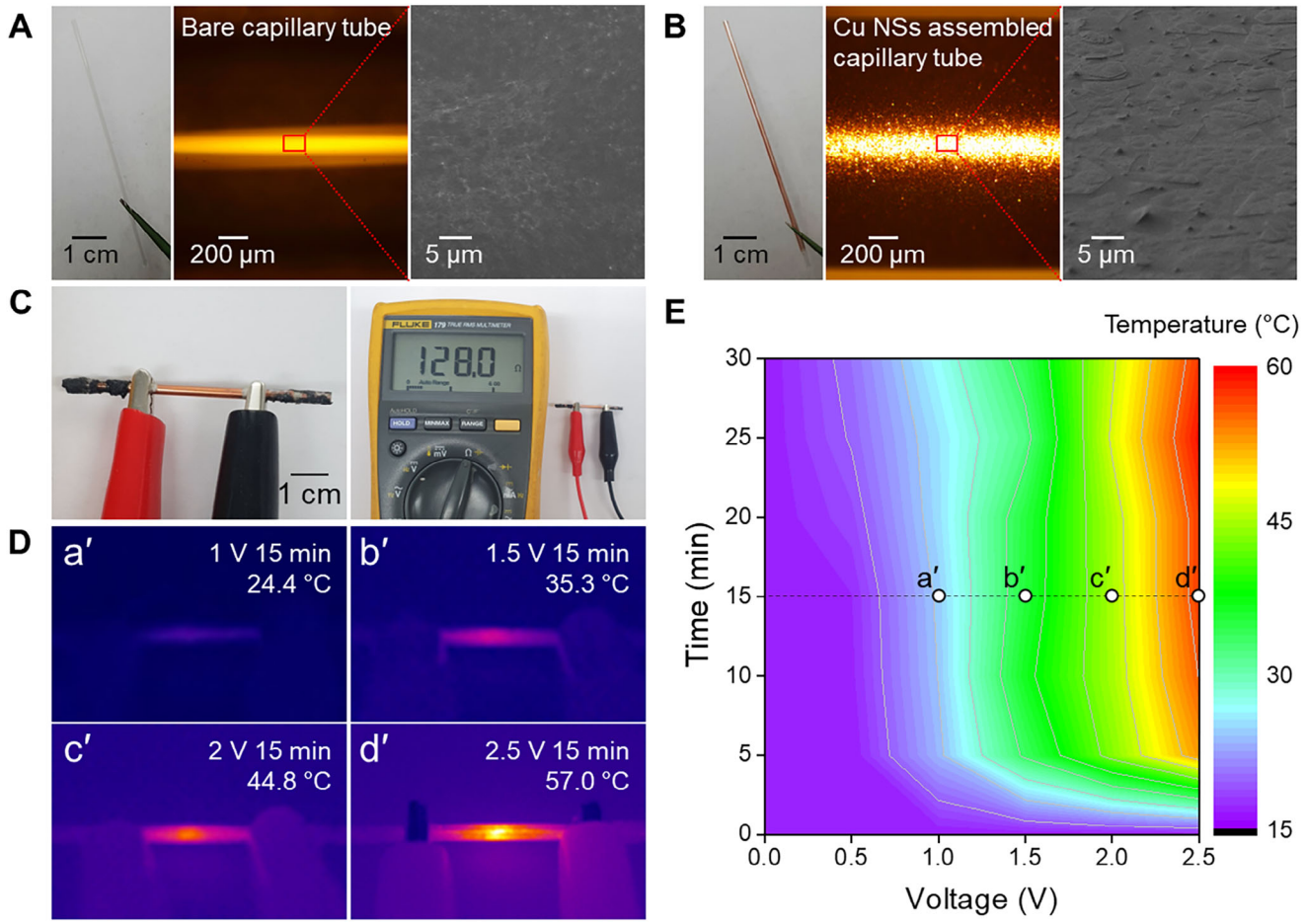

Figure 6. Copper nanosheet (Cu NS)-assembled capillary tube heater. A) A bare glass capillary tube. Optical microscopy (OM) and scanning electron microscopy (SEM) images of an uncoated glass capillary tube. B) Cu NS assembled capillary tube. The OM image displays a consistent layer of Cu NS on the tube's surface, and the SEM image illustrates the dense and uniform assembly of nanosheets, confirming successful coating and coverage. C) Electrical measurement setup of Cu NS assembled capillary tube. The assembled capillary tube exhibits an electrical resistance of ≈128.0 Ω. D) Thermal infrared (IR) images under different applied voltages. IR images depict the temperature distribution along the Cu NS-coated capillary tube at various voltages: (a′) at 1 V with a temperature of 24.4 °C, (b′) at 1.5 V with 35.3 °C, (c′) at 2 V with 44.8 °C, and (d′) at 2.5 V with 57.0 °C. E) A thermal map as a function of the applied voltage and time. The 3D thermal gradient indicates a consistent increase in temperature with both voltage and time, indicating efficient and controllable heating properties of the Cu NS assembly.

at a relatively low voltage of 2.5 V. We also conducted stability tests of the conductive Cu NS films under three different environmental conditions: long-term storage, high humidity exposure, and elevated temperature (Figures S14–S16, Supporting Information). The results clearly demonstrate that the electrical conductivity of the Cu NS films remains stable across all tested conditions, further confirming their environmental robustness and practical applicability. These results suggest that our ultrasonic-driven omni-directional assembly is a promising coating process for forming conductive films on complex 3D structures.

3. Conclusion

We developed a simple and versatile method for omni-directional assembly of 2D single-crystal Cu NS onto substrates of various shapes and complex geometries using ultrasonication. By exploiting the cavitation effects induced by ultrasonic waves, we achieved uniform monolayer films of Cu NS with largely monolayer films with some degree of nanosheet overlap, effectively overcoming the limitations of traditional deposition techniques. The assembly process is influenced by the interplay between the hydrophobic Cu NS, the hydrophilic substrate surface, and solvent choice, with non-polar solvents enhancing adsorption efficiency. Control of the oxidation state of the Cu NS was crucial, as oxidized Cu NS showed poor assembly due to increased roughness and stronger solvent interactions. The method's versatility was demonstrated by successfully coating complex 3D structures, such as capillary tubes. A tube-shaped resistive heater fabricated by assembling Cu NS on a glass capillary tube, showed excellent heating performance at low voltages. This ultrasonic-driven method offers a scalable approach to fabricating conductive films on complex geometries and opens new possibilities for integrating 2D metal nanomaterials into advanced electronic devices and flexible electronics.

4. Experimental Section

Materials: Copper (nanopowder, 25 nm particle size), Copper(II) chloride dihydrate ($CuCl_2{\cdot}2H_2O$, 99.0+%), glucose (D-(+)-Glucose, 99.5+%), hexadecylamine (HDA, 98%), and iodine (I_2, 99.8+%) were purchased from Sigma–Aldrich. The solvents, (CF, 99.5%; IPA, 99.5%; AC, 99.5%; MtOH, 99.5%; and EtOH, 95%), were purchased from Samchun Pure Chemical Industry Co., Ltd. And other solvents, such as n-hexane, toluene, chlorobenzene, dichlorobenzene, acetonitrile, and EG, were also purchased from Sigma–Aldrich. Triple distilled water was prepared from DIW. All materials and solvents were used without further purification. The glass substrate was an XG glass substrate (1.5 cm × 1.5 cm), and the silicon substrate was SiO_2/Si 100 nm substrate (1.5 cm × 1.5 cm).

Preparation of Cu NS: A hydrothermal synthesis method was used to 2D single-crystal copper nanosheets. Various amounts of I_2 were stirred at 75 °C and 1000 rpm to completely dissolve in DIW. This iodide anion solution was mixed with $CuCl_2{\cdot}2H_2O$ (6.3 mg mL^{-1}), glucose (7.3 mg mL^{-1}), and HDA (43.7 mg mL^{-1}) in DI water at room temperature. The prepared mixed solution was allowed to react at 100 °C for 12 h in an autoclave. After the reaction, the solution containing Cu NS was carefully purified by several centrifugation steps using hot DIW and CF to separate the Cu NS. The Cu NS powder was then recovered using a polytetrafluoroethylene (PTFE) membrane filter (47 mm in diameter, 0.5 µm pore size, Advantec, Japan).

Preparation of Substates: To assemble a monolayer film of copper nanosheets, a glass substrate was initially cleaned of dust particles using DIW followed by ultrasonic cleaning in AC, MtOH, and IPA for 10 min each. The remaining solvent was dried using an air gun. To remove any residual contaminants and induce superhydrophilicity, UV-ozone treatment was performed for 10 min using 254 nm UV light. Silicon wafers, PI film, and Teflon substrates underwent the same cleaning process, except for the DIW rinse. The 3D glass structures with complex designs (e.g., teapots, cubes, pumpkins, and whales) were dried in an oven at 70 °C for 20 min after cleaning.

Assembly Process of Cu NS: Purified copper nanosheets were filtered and dried to obtain copper nanosheet powder. The desired solvent was added to this powder, and it was fully redispersed using an ultrasonicator (UCP-10, Jeiotech). For this pportion of the experiment n-hexane, toluene, chlorobenzene (CB), CF, DCB were used as non-polar solvents, while IPA, AC, EtOH, MtOH, ACN, DIW, and EG were used as polar solvents. To determine the effect of ultrasonic-driven assembly on polar and non-polar solvents, 6 mg of Cu NS powder was dispersed in 2 mL of each of the solvents to prepare 3 mg mL^{-1} Cu NS solutions based on various solvents, and ultrasonic-driven assembly was performed. Due to the hydrophobicity of copper nanosheets, a vortex mixer was also used to aid dispersion in deionized water. Cu NS solutions with concentrations of 1 , 3 , 5 , 7 , 9 , and 11 mg mL^{-1} were prepared by adjusting the amount of Cu NS powder and dispersing it in CF. The prepared substrate and Cu NS solution were placed in a 20 mL vial and fixed in an ultrasonicator. The ultrasonicator (Jeiotech UCP-10) emitted 40 kHz ultrasonic waves, and the process time was controlled using its built-in timer. After assembly, the substrate was removed from the vial, rinsed with the same solvent used for dispersion to remove excess Cu NS, and the remaining solvent was dried on a hot plate at 70 °C. To verify the application to various substrate effect, in addition to glass and SiO2/Si substrates, PI film, Teflon, a glass optical fiber, a glass capillary tube, a glass teapot, a glass pumpkin, a glass whale, dice-patterned glass, and polyethylene naphthalate were prepared by washing them in AC, MtOH, and IPA, respectively, and ultrasonic-driven assembly was performed using the same process as mentioned earlier. To evaluate the assembly of Cu NS on the substrate, images were taken at five different points on each film using an optical microscope (S39A, Microscopes Inc.), and the average surface coverage was calculated using ImageJ software. The Cu NS film and individual Cu NS were analyzed by field emission scanning electron microscopy (FE-SEM, Gemini 500, Carl Zeiss, Germany) at the Center for University-wide Research Facilities at Jeonbuk National University. Contact angles were measured using a goniometer (Phoenix 300, SEO) and 5 µL of DIW.

Selective Assembly of Cu NS: An Al_2O_3 thin film was first deposited on cleaned glass and SiO_2/Si substrates. Al_2O_3 films were deposited by RF (13.56 MHz) magnetron sputtering, using an Al_2O_3 (99.95% purity) target with a diameter of 2 inches under a pressure of 0.67 Pa and a 20 sccm flow of argon (99.999%) gas. The RF input power and substrate temperature were kept at 150 W and room temperature, respectively. The deposited films were ≈30 nm thick, and the argon flow rate was controlled by mass flow controllers. Al_2O_3/glass or Al_2O_3/SiO_2/Si substrates were then treated with UV-ozone for 10 min, sealed in a 0.5 mM FDDPA solution, and heated to 50 °C. The FDDPA solution (0.314 mg mL^{-1}) was prepared by dissolving FDDPA in ethanol and filtering it through a 0.2 µm PTFE filter. After 48 h, the substrate was removed from the solution and washed with ethanol, leaving the surface covered with FDDPA SAM, making it hydrophobic. The surface of the substrate was modified to become hydrophobic by forming a self-assembled layer of (3,3,4,4,5,5,6,6,7,7,8,8,9,9,10,10,11,11,12,12,12-Heneicosafluorododecyl) phosphonic acid (FDDPA). To create hydrophilic patterning on the hydrophobic substrate covered with the FDDPA SAM layer, a shadow mask was applied, and UV/ozone was irradiated through the shadow mask for 5 min, making the exposed area hydrophilic. Finally, the prepared substrate and Cu NS mixture solution were placed in a 20 mL vial in an ultrasonic cleaner for ultrasonic-driven assembly of Cu NS on the desired surface.

Fabrication of Cu NS–Based 3D Heater: To fabricate a tube-type heater, a plain capillary tube (75 mm ± 0.5 mm, 1.1–1.2 mm inner diameter, 1.5–1.6 mm outer diameter, Marienfeld Superior, Lauda-Königshofen, Germany) was cleaned with AC, MtOH, and IPA using an ultrasonicator for 10 min each. The remaining solvent was then dried in an oven at 70 °C for 20 min, followed by UV-ozone treatment at a wavelength of 254 nm. Prior to the ultrasonic-driven assembly of Cu NS, both tube inlets were sealed with Teflon tape to prevent internal coating. The tube was then placed in a solution of Cu NS dispersed in chloroform, and ultrasonic waves were applied. After ultrasonic-driven assembly, the tube was removed from the solution, excess solvent was absorbed using a disposable Science Wiper, and the tube was dried in an oven at 70 °C for 1 min. Before evaluating the electrical and heat generation properties, heat treatment was performed for 1 g in an Ar/H_2 (95:5) atmosphere at 250 °C to enhance bonding between sheets. To facilitate evaluation, both tube ends were coated with silver paste (ELCOAT P-100, CANS, Japan), and alligator clips were attached. Resistance was measured using a Fluke 179 True RMS multimeter. To analyze the heating performance of the Cu NS–assembled tube, DC voltages of 0.5 , 1 , 1.5 , 2 , and 2.5 V were applied for 30 min using a KEYSIGHT 33500B waveform generator, while heating was monitored using a Testo 875 thermal imager (Testo 875i basic, Germany).

Supporting Information

Supporting Information is available from the Wiley Online Library or from the author.

Acknowledgements

This work was supported by the National Research Foundation of Korea (RS-2024-00452255, RS-2022-NR068320) and also supported by the Commercialization Promotion Agency for R&D Outcomes(COMPA) grant funded by the Korean Government (Ministry of Science and ICT). (RS-2023-00304743).

Conflict of Interest

The authors declare no conflict of interest.

Data Availability Statement

The data that support the findings of this study are available from the corresponding author upon reasonable request.

Keywords

2D metallic nanomaterials, conductive thin films, omni-directional assembly, single-crystalline metal nanosheet, ultrasonic-driven assembly

Received: January 23, 2025
Revised: March 11, 2025
Published online: March 27, 2025

[1] T. Cheng, Y. Zhang, W. Y. Lai, W. Huang, *Adv. Mater.* **2015**, *27*, 3349.
[2] J. A. Rogers, T. Someya, Y. Huang, *Science* **2010**, *327*, 1603.
[3] T. Sannicolo, M. Lagrange, A. Cabos, C. Celle, J. P. Simonato, D. Bellet, *Small* **2016**, *12*, 6052.
[4] D. S. Hecht, L. Hu, G. Irvin, *Adv. Mater.* **2011**, *23*, 1482.
[5] Q. Cao, J. A. Rogers, *Adv. Mater.* **2009**, *21*, 29.
[6] Y. Shi, L. Peng, Y. Ding, Y. Zhao, G. Yu, *Chem. Soc. Rev.* **2015**, *44*, 6684.
[7] C. Wang, C. Wang, Z. Huang, S. Xu, *Adv. Mater.* **2018**, *30*, 1801368.
[8] J. Kang, W. Cao, X. Xie, D. Sarkar, W. Liu, K. Banerjee, presented at Micro-and Nanotechnology Sensors, Systems, and Applications VI, SPIE, Bellingham, WA **2014**.
[9] A. Baptista, F. Silva, J. Porteiro, J. Míguez, G. Pinto, *Coatings* **2018**, *8*, 402.
[10] W. D. Sproul, *Surf. Coat. Technol.* **1996**, *81*, 1.
[11] M. A. Butt, *Coatings* **2022**, *12*, 1115.
[12] Y. Kim, S. Jang, J. H. Oh, *Appl. Phys. Lett.* **2015**, *106*, 014103.
[13] M. S. Onses, E. Sutanto, P. M. Ferreira, A. G. Alleyne, J. A. Rogers, *Small* **2015**, *11*, 4237.
[14] H. Wu, L. Hu, M. W. Rowell, D. Kong, J. J. Cha, J. R. McDonough, J. Zhu, Y. Yang, M. D. McGehee, Y. Cui, *Nano Lett.* **2010**, *10*, 4242.
[15] Q. Huang, Y. Zhu, *Adv. Mater. Technol.* **2019**, *4*, 1800546.
[16] J. A. Lim, W. H. Lee, H. S. Lee, J. H. Lee, Y. D. Park, K. Cho, *Adv. Funct. Mater.* **2008**, *18*, 229.
[17] Y. Huang, H. Wu, L. Xiao, Y. Duan, H. Zhu, J. Bian, D. Ye, Z. Yin, *Mater. Horiz.* **2019**, *6*, 642.
[18] S. Khan, L. Lorenzelli, R. S. Dahiya, *IEEE Sens. J.* **2014**, *15*, 3164.
[19] J. W. Jo, J. W. Jung, J. U. Lee, W. H. Jo, *ACS Nano* **2010**, *4*, 5382.
[20] F. Mirri, A. W. Ma, T. T. Hsu, N. Behabtu, S. L. Eichmann, C. C. Young, D. E. Tsentalovich, M. Pasquali, *ACS Nano* **2012**, *6*, 9737.
[21] S. An, B. Joshi, A. L. Yarin, M. T. Swihart, S. S. Yoon, *Adv. Mater.* **2020**, *32*, 1905028.
[22] A. Kamyshny, M. Ben-Moshe, S. Aviezer, S. Magdassi, *Macromol. Rapid Commun.* **2005**, *26*, 281.
[23] L. Ye, Y. Xiong, H. Yao, A. Gadisa, H. Zhang, S. Li, M. Ghasemi, N. Balar, A. Hunt, B. T. O'Connor, J. Hou, H. Ade, *Chem. Mater.* **2016**, *28*, 7451.
[24] S. Z. Butler, S. M. Hollen, L. Cao, Y. Cui, J. A. Gupta, H. R. Gutiérrez, T. F. Heinz, S. S. Hong, J. Huang, A. F. Ismach, E. J. Halperin, M. Kuno, V. V. Plashnitsa, R. D. Robinson, R. S. Ruoff, S. Salahuddin, J. Shan, L. Shi, M. G. Spencer, M. Terrones, W. Windl, J. E. Goldberger, *ACS Nano* **2013**, *7*, 2898.
[25] M. Chhowalla, H. S. Shin, G. Eda, L.-J. Li, K. P. Loh, H. Zhang, *Nat. Chem.* **2013**, *5*, 263.
[26] M. Xu, T. Liang, M. Shi, H. Chen, *Chem. Rev.* **2013**, *113*, 3766.
[27] S. Manzeli, D. Ovchinnikov, D. Pasquier, O. V. Yazyev, A. Kis, *Nat. Rev. Mater.* **2017**, *2*, 17033.
[28] K. S. Novoselov, D. Jiang, F. Schedin, T. Booth, V. Khotkevich, S. Morozov, A. K. Geim, *Proc. Natl. Acad. Sci. USA* **2005**, *102*, 10451.
[29] C. Tan, X. Huang, H. Zhang, *Mater. Today* **2013**, *16*, 29.
[30] R. Lv, J. A. Robinson, R. E. Schaak, D. Sun, Y. Sun, T. E. Mallouk, M. Terrones, *Acc. Chem. Res.* **2015**, *48*, 56.
[31] Y. Chen, Z. Fan, Z. Zhang, W. Niu, C. Li, N. Yang, B. Chen, H. Zhang, *Chem. Rev.* **2018**, *118*, 6409.
[32] Z. Sun, T. Liao, Y. Dou, S. M. Hwang, M.-S. Park, L. Jiang, J. H. Kim, S. X. Dou, *Nat.Commnun.* **2014**, *5*, 3813.
[33] J. W. Lee, J. Han, D. S. Lee, S. Bae, S. H. Lee, S. K. Lee, B. J. Moon, C. J. Choi, G. Wang, T. W. Kim, *Small* **2018**, *14*, 1703312.
[34] H. K. Choi, A. Lee, M. Park, D. S. Lee, S. Bae, S.-K. Lee, S. H. Lee, T. Lee, T.-W. Kim, *ACS Nano* **2021**, *15*, 829.
[35] M. B. Gawande, A. Goswami, F.-X. Felpin, T. Asefa, X. Huang, R. Silva, X. Zou, R. Zboril, R. S. Varma, *Chem. Rev.* **2016**, *116*, 3722.
[36] Y. Shi, Z. Lyu, M. Zhao, R. Chen, Q. N. Nguyen, Y. Xia, *Chem. Rev.* **2020**, *121*, 649.
[37] C. Liang, Z. Gu, Y. Zhang, Z. Ma, H. Qiu, J. Gu, *Nanomicro Lett.* **2021**, *13*, 181.
[38] S. M. Jafari, Y. He, B. Bhandari, *Int. J. Food Prop.* **2006**, *9*, 475.
[39] A. V. Tyurnina, I. Tzanakis, J. Morton, J. Mi, K. Porfyrakis, B. M. Maciejewska, N. Grobert, D. G. Eskin, *Carbon* **2020**, *168*, 737.
[40] R. N. Weller, J. M. Brady, W. E. Bernier, *J. Endod.* **1980**, *6*, 740.
[41] D. Y. Hoo, Z. L. Low, D. Y. S. Low, S. Y. Tang, S. Manickam, K. W. Tan, Z. H. Ban, *Ultrason. Sonochem.* **2022**, *90*, 106176.
[42] F. Laugier, C. Andriantsiferana, A.-M. Wilhelm, H. Delmas, *Ultrason. Sonochem.* **2008**, *15*, 965.
[43] E. A. Neppiras, *Phys. Rep.* **1980**, *61*, 159.
[44] J. Carpenter, M. Badve, S. Rajoriya, S. George, V. K. Saharan, A. B. Pandit, *Rev. Chem. Eng.* **2017**, *33*, 433.
[45] C. Sauter, M. Emin, H. Schuchmann, S. Tavman, *Ultrason. Sonochem.* **2008**, *15*, 517.
[46] H. K. Choi, S. Bae, S.-K. Lee, S. H. Lee, K. Lee, S.-Y. Ko, J.-W. Kang, S.-Y. Yang, T.-W. Kim, *Mater. Sci. Eng. B* **2022**, *278*, 115611.
[47] D. V. R. Kumar, A. M. Koshy, N. Sharma, N. Thomas, P. Swaminathan, *ACS Omega* **2023**, *8*, 21107.
[48] B. Ha, S. Jo, *Sci. Rep.* **2017**, *7*, 11614.
[49] H.-C. Chu, Y.-C. Chang, Y. Lin, S.-H. Chang, W.-C. Chang, G.-A. Li, H.-Y. Tuan, *ACS Appl. Mater. Interfaces.* **2016**, *8*, 13009.
[50] S. Polat Genlik, D. Tigan, Y. Kocak, K. E. Ercan, M. O. Cicek, S. Tunca, S. Koylan, S. Coskun, E. Ozensoy, H. E. Unalan, *ACS Appl. Mater. Interfaces.* **2020**, *12*, 45136.
[51] N. Bharadishettar, U. Bhat K, D. Bhat Panemangalore, *Metals* **2021**, *11*, 711.
[52] S.-J. Joo, S.-H. Park, C.-J. Moon, H.-S. Kim, *ACS Appl. Mater. Interfaces.* **2015**, *7*, 5674.
[53] J. S. Kang, H. S. Kim, J. Ryu, H. Thomas Hahn, S. Jang, J. W. Joung, *J. Mater. Sci. Mater. Electron.* **2010**, *21*, 1213.
[54] S.-H. Park, W.-H. Chung, H.-S. Kim, *J. Mater. Process. Technol.* **2014**, *214*, 2730.
[55] M. Kanwal, X. Wang, H. Shahzad, Y. Chen, H. Chai, *J. Plast. Film Sheeting* **2020**, *36*, 348.
[56] J. R. Blake, D. Gibson, *Annu. Rev. Fluid Mech.* **1987**, *19*, 99.
[57] C. E. Brennen, *Cavitation and Bubble Dynamics*, Cambridge University Press, Cambridge, UK **2014**.
[58] A. Philipp, W. Lauterborn, *J. Fluid Mech.* **1998**, *361*, 75.
[59] D. G. Shchukin, E. Skorb, V. Belova, H. Möhwald, *Adv. Mater.* **2011**, *23*, 1922.
[60] S. R. Gonzalez-Avila, D. M. Nguyen, S. Arunachalam, E. M. Domingues, H. Mishra, C.-D. Ohl, *Sci. Adv.* **2020**, *6*, aax6192.
[61] F. W. DelRio, M. P. De Boer, J. A. Knapp, E. David Reedy Jr, P. J. Clews, M. L. Dunn, *Nat. Mater.* **2005**, *4*, 629.
[62] X. Xu, J.-W. He, D. W. Goodman, *Surf. Sci.* **1993**, *284*, 103.
[63] Y. L. Chen, S. Chen, C. Frank, J. Israelachvili, *J. Colloid Interface Sci.* **1992**, *153*, 244.
[64] D. K. Schwartz, *Annu. Rev. Phys. Chem.* **2001**, *52*, 107.
[65] M. N. Martin, J. I. Basham, P. Chando, S.-K. Eah, *Langmuir* **2010**, *26*, 7410.
[66] J. Jiménez-Lamana, V. I. Slaveykova, *Sci. Total Environ.* **2016**, *573*, 946.
[67] R. A. Erb, *J. Phys. Chem.* **1965**, *69*, 1306.

[68] D. Zhu, Z. Shi, X. Tan, J. Zhang, S. Zhang, X. Zhang, *Appl. Surf. Sci.* **2020**, *527*, 146741.
[69] I. Platzman, R. Brener, H. Haick, R. Tannenbaum, *J. Phys. Chem. C* **2008**, *112*, 1101.
[70] S. J. Kim, Y. I. Kim, B. Lamichhane, Y.-H. Kim, Y. Lee, C. R. Cho, M. Cheon, J. C. Kim, H. Y. Jeong, T. Ha, J. Kim, Y. H. Lee, S.-G. Kim, Y.-M. Kim, S.-Y. Jeong, *Nature* **2022**, *603*, 434.
[71] A. Soon, M. Todorova, B. Delley, C. Stampfl, *Phys. Rev. B* **2006**, *73*, 165424.
[72] T. Delchar, *Surf. Sci.* **1971**, *27*, 11.
[73] F. Wiame, V. Maurice, P. Marcus, *Surf. Sci.* **2007**, *601*, 1193.
[74] S. Yamamoto, K. Andersson, H. Bluhm, G. Ketteler, D. E. Starr, T. Schiros, H. Ogasawara, L. G. Pettersson, M. Salmeron, A. Nilsson, *J. Phys. Chem. C* **2007**, *111*, 7848.
[75] R. L. DeRosa, P. A. Schader, J. E. Shelby, *J. Non-Cryst. Solids* **2003**, *331*, 32.
[76] D. Okhrimenko, C. Nielsen, L. Lakshtanov, K. Dalby, D. Johansson, M. Solvang, J. Deubener, S. Stipp, *ACS Appl. Mater. Interfaces.* **2020**, *12*, 36740.
[77] M. K. Bernett, W. Zisman, *J. Colloid Interface Sci.* **1969**, *29*, 413.
[78] A. Rimola, D. Costa, M. Sodupe, J.-F. Lambert, P. Ugliengo, *Chem. Rev.* **2013**, *113*, 4216.
[79] M. R. Basila, *J. Chem. Phys.* **1961**, *35*, 1151.
[80] M. Virot, T. Chave, S. I. Nikitenko, D. G. Shchukin, T. Zemb, H. Möhwald, *J. Phys. Chem. C* **2010**, *114*, 13083.
[81] Z. Zuo, W. Huang, P. Han, Z. Li, *Appl. Surf. Sci.* **2010**, *256*, 2357.
[82] R. Ferullo, G. R. Garda, P. G. Belelli, M. M. Branda, N. J. Castellani, *J. Mol. Struct.: THEOCHEM* **2006**, *769*, 217.
[83] A. De Lazzer, M. Dreyer, H. Rath, *Langmuir* **1999**, *15*, 4551.
[84] Z. Jian-Min, M. Fei, X. Ke-Wei, *Chin. Phys.* **2004**, *13*, 1082.
[85] N. Bunkin, O. Kiseleva, A. Lobeyev, T. Movchan, B. Ninham, O. Vinogradova, *Langmuir* **1997**, *13*, 3024.
[86] N. Bremond, M. Arora, S. M. Dammer, D. Lohse, *Phys. Fluids* **2006**, *18*, 121505.
[87] N. Bremond, M. Arora, C.-D. Ohl, D. Lohse, *Phys. Rev. Lett.* **2006**, *96*, 224501.
[88] V. Belova-Magri, A. Brotchie, C. Cairos, R. Mettin, H. Mohwald, *ACS Appl. Mater. Interfaces.* **2015**, *7*, 4100.
[89] V. Belova, D. A. Gorin, D. G. Shchukin, H. Möhwald, *ACS Appl. Mater. Interfaces.* **2011**, *3*, 417.
[90] V. F. Humphrey, *Prog. Biophys. Mol. Biol.* **2007**, *93*, 195.
[91] M. J. Vellekoop, *Ultrasonics* **1998**, *36*, 7.
[92] H. Wu, Y. Tian, H. Luo, H. Zhu, Y. Duan, Y. Huang, *Adv. Mater. Technol.* **2020**, *5*, 2000093.